SLAC−PUB−10170

# PERFORMANCE AND CALIBRATION OF THE CRYSTAL CALORIMETER OF THE BABAR DETECTOR

M. KOCIAN

*SLAC, MS 61, 2575 Sand Hill Rd.,Menlo Park, CA 94025, USA*
*E-mail: kocian@slac.stanford.edu*

*(for the BABAR calorimeter group)*

The *BABAR* detector at the B-factory at SLAC is equipped with a calorimeter consisting of 6580 CsI(Tl) crystals. This allows for the measurement of the energies of photons and neutral pions and the identification of electrons with high precision, needed in the reconstruction of B-meson decays. The detailed performance of the calorimeter will be presented. As the B-factory operates at high luminosity the calorimeter is exposed to substantial background and radiation damage. The calorimeter is calibrated regularly at different energies in order to meet the precision goals. The calibration methods include the use of a radioactive source, Bhabha events, radiative Bhabha events, $\pi^0$-Mesons, and a light pulser system. This article largely follows reference[1].

## 1. Introduction

*BABAR* is the detector at the PEP-II $B$ Factory at SLAC. PEP-II is an asymmetric $e^+e^-$-collider, currently operating at a luminosity of $4.5 \times 10^{33}$ $\mathrm{cm}^{-2}\mathrm{s}^{-1}$ at a center-of-mass energy of 10.58 GeV, the mass of the $\Upsilon(4S)$ resonance. The $\Upsilon(4S)$ decays exclusively into $B^0\bar{B}^0$ and $B^+B^-$ pairs. The main physics goal of *BABAR* is the study of $CP$-violating asymmetries in the decay of neutral $B$-mesons. Secondary goals are precision measurements of decays of bottom and charm mesons and of $\tau$ leptons, and searches for rare processes that become accessible with the high luminosity of the PEP-II $B$ Factory. The *BABAR* detector consists of 6 subdetectors. From the inside to the outside, there is a Silicon Vertex Detector, a Drift Chamber, a DIRC (Cherenkov- Detector), an Electromagnetic Calorimeter, and an Instrumented Flux Return (fig. 1).

## 2. Calorimetry goals

The very small branching ratios of $B$ mesons to $CP$ eigenstates and the need for full reconstruction of final states with several $\pi^0$s place stringent requirements



Work supported in part by the Department of Energy contract DE−AC03−76SF00515.
Stanford Linear Accelerator Center, Stanford University, Stanford, CA 94309

Presented at the 10th International Conference on
Calorimetry in High Energy Physics (CALOR 2002), Pasadena, CA, March 25−29, 2002

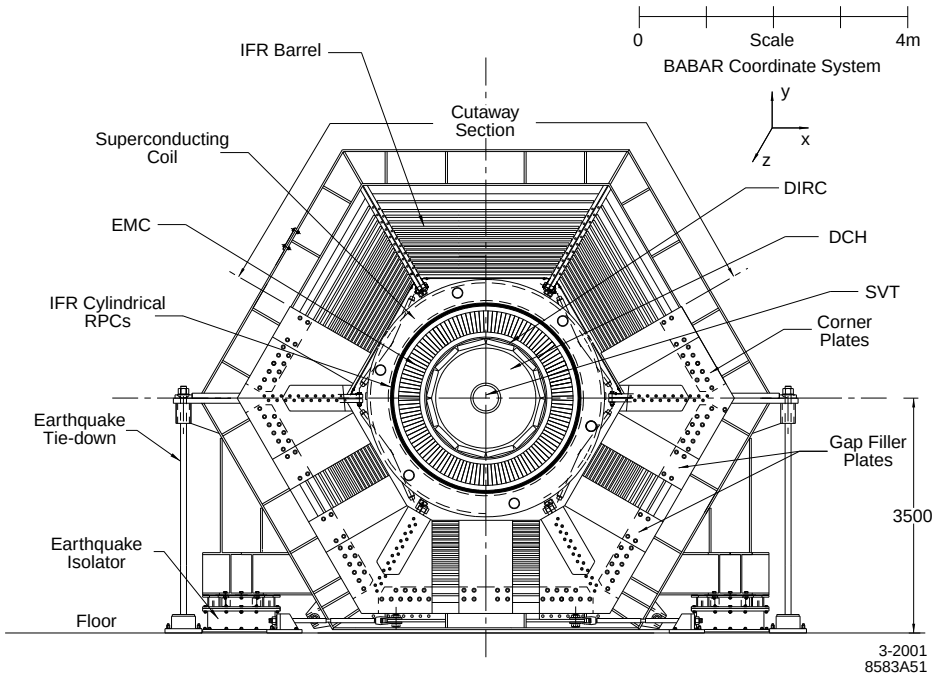


Figure 1. The components of the $BABAR$ detector

on the electromagnetic calorimeter:

- a large and uniform acceptance down to small polar angles relative to the boost direction
- excellent reconstruction efficiency for photons down to 20 MeV
- energy resolution of order $1-2$ % and excellent angular resolution for the detection of photons from $\pi^0$ and $\eta$ decays in the range from 20 MeV to 4 GeV
- efficient electron identification with low misidentification probabilities for hadrons.

For these reasons the choice for $BABAR$ was a CsI(Tl) crystal calorimeter. The energy resolution of a homogeneous crystal calorimeter can be described empirically in terms of a sum of two terms added in quadrature

$$\frac{\sigma_E}{E} = \frac{a}{\sqrt[4]{E(\mathrm{GeV})}} \oplus b, \tag{1}$$

where $E$ and $\sigma_E$ refer to the energy of a photon and its rms error, measured in GeV. The energy dependent term $a$ arises from fluctuations in photon statistics,

electronics noise and beam background noise. The constant term $b$ is dominant at higher energies and arises from non-uniformity in light collection, shower leakage or absorption in the material between and in front of the crystals, and uncertainties in calibration. The angular resolution is determined from the transverse crystal size and the distance from the interaction point. It is parametrized as

$$\sigma_\theta = \sigma_\phi = \frac{c}{\sqrt{E(\mathrm{GeV})}} + d, \tag{2}$$

The actual resolution for the *BABAR* calorimeter will be discussed in section 5.2.

## 3. Layout and Assembly

### 3.1. *General Overview*

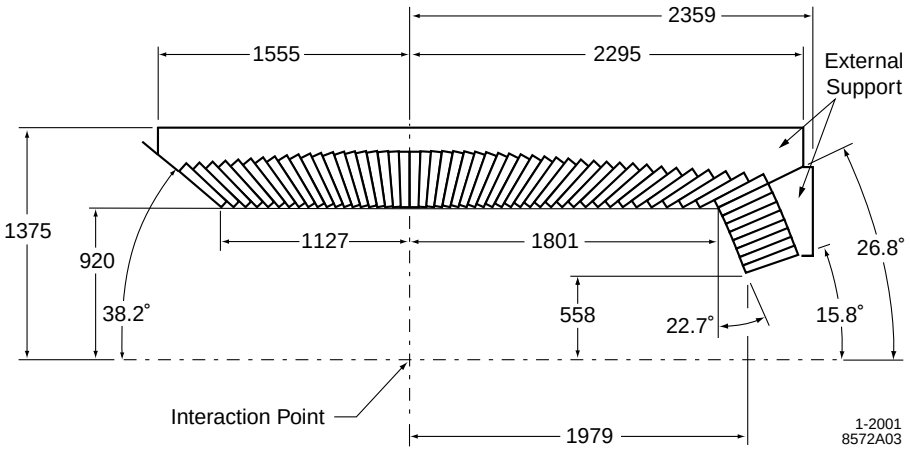


Figure 2. A longitudinal cross-section of the Calorimeter

The calorimeter consists of 6580 CsI(Tl) crystals. Its angular coverage is 126° in polar angle and 360° in azimuthal angle (see fig. 2). It is subdivided into a barrel and a forward endcap. The barrel consists of 5760 crystals arranged in 48 rings of 120 crystals, while the endcap contains 8 rings. The innermost 2 rings contain 80 crystals, the next three rings 100, and the three outer rings 120 crystals. The calorimeter's geometry is projective in $\phi$, while in $\theta$ there is a non-projectivity of 14 mrad, except in the transition region between barrel and endcap where it reaches 45 mrad. The non-projectivity minimizes the

energy losses through the spaces between the crystals. There is a gap of about 2 mm between the barrel and the endcap which is fully covered by the higher non-projectivity in this region.

### 3.2. *Mechanical Assembly*

The individual crystals are assembled in carbon fiber modules. In the barrel, the modules contain 7 x 3 crystals (except for the most backward module which only contains 6 x 3 crystals). The entire barrel consists of 280 carbon fiber modules. In the endcap, each carbon fiber module contains 41 crystals. The carbon fiber housings are glued onto Aluminum strongbacks. The barrel modules are inserted into an Aluminum cylinder. The endcap modules are held in place by two semicircular structures.

### 3.3. *Crystal Assembly*

The crystals are trapezoidal in shape. The typical area of the front face is 4.7 x 4.7 $cm^2$, while the back face area is typically 6.1 x 6.0 $cm^2$. The length of the crystals varies between 16 radiation lengths in the backward part and 17.5 radiation lengths in the forward part. The polished crystals are wrapped in two layers of Tyvek (2 x 165 $\mu$m) for reflection and tuning. The next layers are Aluminum foil (25 $\mu$m) and Mylar (13 $\mu$m) for electrical insulation (fig. 3). The outside layer is a 300 $\mu$m thick carbon fiber housing which is attached to the housings of the neighbour crystals. The crystals are read out through 2 silicon PIN photodiodes of 2 x 1 $cm^2$ area each. The diodes are glued onto a polystyrene coupling plate which itself is glued onto the crystal with transparent epoxy. The area surrounding the diodes is covered with white, painted plastic plates to reflect light. Each diode is read out by a preamplifier that sits in a housing above the crystal. For the details of the electronics readout see reference[2].

## 4. Calibration

### 4.1. *Overview*

The energy calibration of the calorimeter proceeds in two steps. First, the measured pulse height in each crystal has to be transformed into the deposited energy. Second, the deposited energy in a shower has to be related to the energy of the incident photon or electron by correcting for energy loss mostly due to leakage and absorption in material between and in front of the crystals. Table 1 shows a summary of the calibrations used for the $BABAR$ calorimeter. The electronics and light pulser calibrations are discussed in reference[2].

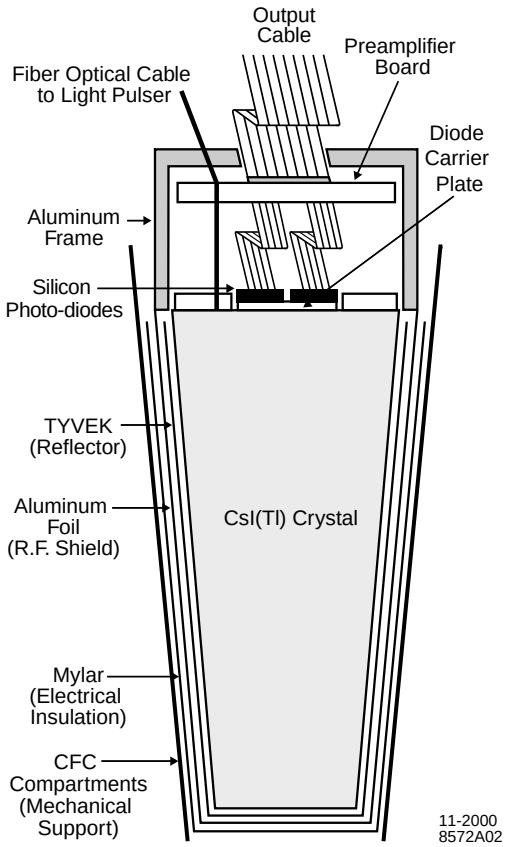


Figure 3. A schematic of the wrapped crystal

Table 1. Properties of the different calibrations for the calorimeter. "Absolute" refers to the ability to tie the measurement to an absolute energy scale as opposed to measuring the relative changes and differences in signal height.

| | Duration | Energy Scale | Single Crystal | Absolute |
|---|---|---|---|---|
| Source | 20 min | 0.00613 GeV | Yes | Yes |
| Bhabha | 12 h | 3-9 GeV | No | Yes |
| $\pi^0$ | 4 h | 0.03 - 3 GeV | No | Yes |
| Electronics | 15 min | 0 - 13 GeV | Yes | No |
| Light Pulser | 3 min | 0 - 13 GeV | Yes | No |

### 4.2. *Individual Crystal Calibration*

In spite of the careful selection and tuning of the crystals, their light yield varies significantly and is non-uniform along the crystal axis. It also changes with time under the impact of beam-generated radiation. The absorbed dose is largest at the front of the crystal and results in increased attenuation of the transmitted scintillation light. The light yield must therefore be calibrated at different energies, corresponding to different average shower penetration, to account for the effects of the radiation damage[3]. The calibration of the deposited energies is performed at two energies at opposite ends of the dynamic range, and these two measurements are combined by a logarithmic interpolation. A 6.13 MeV radioactive photon source provides an absolute calibration at low energy, while at higher energies the relation between polar angle and energy in Bhabha events is used for calibration.

#### 4.2.1. *Radioactive Source Calibration*

The radioactive source calibration uses 6.13 MeV photons produced in the reaction

$$^{19}F + n \rightarrow^{16} N + \alpha,^{16} N \rightarrow^{16} O^* + \beta,^{16} O^* \rightarrow^{16} O + \gamma. \quad (3)$$

$^{16}N$ has a lifetime of 7 seconds. A fluid of polychlorotrifluoro-ethylene, activated by neutrons from a generator, circulates through a system of tubes in front of the crystals. All crystals in the calorimeter are calibrated with this method. The average resolution for the constants is 0.33 %.

#### 4.2.2. *The Bhabha Calibration*

At high energies, single crystal calibration is performed with a pure sample of Bhabha events. As a function of the polar angle of the $e^{\pm}$, the deposited cluster energy is constrained to equal the prediction of a GEANT based Monte Carlo simulation. For a large number of energy clusters, a set of simulates linear equations relates the measured to the expected energy and thus permits the determination of a constant for each crystal. 200 $e^{\pm}$ per crystal result in constants with a statistical error of 0.35 %.

### 4.3. *Shower Energy Correction*

The correction for energy loss due to shower leakage and absorption is performed as a function of shower energy and polar angle. For low energies it is derived from $\pi^0$ decays, while for high energies corrections derived from single photon Monte Carlo or from radiative Bhabha events can be used.

#### 4.3.1. $\pi^0$ *Calibration*

For the $\pi^0$ calibration the energy range is subdivided into 16 bins in $\ln(E)$, while the angular range is divided into 9 bins in $\cos(\theta)$. For each bin a two-photon-mass plot is generated. By constraining the peaks to the nominal mass, a correction polynomial of third order in $\ln(E)$ and a correction polynomial of second order in $\cos(\theta)$ are determined in an iterative procedure. Typical corrections are of order $6 \pm 1$ %.

## 5. Performance

### 5.1. $\pi^0$ *and* $\eta$ *mass and width*

Figure 4a shows the two-photon invariant mass for hadronic events around the $\pi^0$ mass in data from 2001. Photons are required to exceed 30 MeV, while $\pi^0$ exceed 300 MeV. The reconstructed mass is measured to be 134.9 MeV/c$^2$. The width is 6.5 MeV/c$^2$. The two-photon-invariant mass for symmetric $\eta$s for $E_\eta > 1$ GeV is shown in figure 4b. The reconstructed mass is 547 MeV/c$^2$, the width is 15.5 MeV/c$^2$.

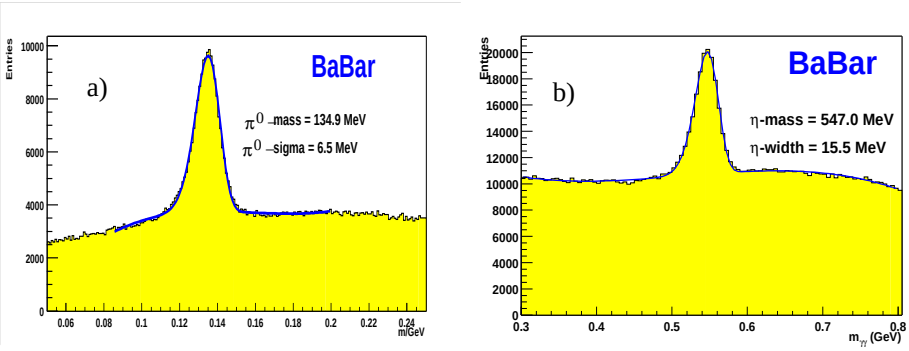


Figure 4. Invariant mass of two photons in hadronic events. The solid lines are fits to the data.

### 5.2. *Resolution*

Figure 5a shows the energy resolution derived from a variety of processes: radioactive source, symmetric $\pi^0$ and $\eta$ decays, $\chi_{c1} \to J/\psi\gamma$, and Bhabha events. As the resolution of $\pi^0$ and $\eta$ depends on the angular resolution also, a simultaneous fit to energy and angular resolution was done for those cases, assuming an asymmetry of the photon energy distribution derived from Monte Carlo. There is good agreement between the measured resolution and Monte

Carlo prediction. The data point from the radioactive source calibration shows a deviation from the fitted curve, as the photons from the radioactive source develop in single crystals and do not traverse material in front of the crystals. The angular resolution derived from symmetric $\pi^0$ and $\eta$ decays is shown in fig. 5b. There is good agreement between the measured resolution and Monte Carlo predictions. Fits to the data yield

$$\frac{\sigma_E}{E} = \frac{(2.30 \pm 0.03 \pm 0.3)\%}{\sqrt[4]{E(\mathrm{GeV})}} \oplus (1.35 \pm 0.08 \pm 0.2)\%, \tag{4}$$

$$\sigma_\theta = \sigma_\phi = \frac{(4.16 \pm 0.04)\mathrm{mrad}}{\sqrt{E(\mathrm{GeV})}} + (0.0 \pm 0.0)\mathrm{mrad}. \tag{5}$$

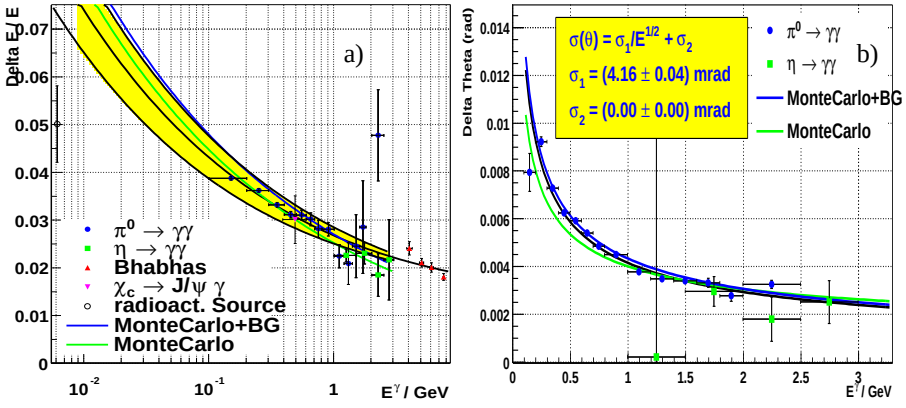


Figure 5. Energy resolution (a) and angular resolution (b). The central black line is a fit to the data points. The outer black lines in (a) show the systematic uncertainty.

## 6. Summary

The Electromagnetic Calorimeter has been working reliably for the past 2.5 years. Its performance has been improved by updates of hardware and software and is close to expectations. The calibrations that have been developed play a crucial role in the performance.

## References

1. *BABAR* Collaboration, *Nucl. Inst. Meth.* **A479**, 1 (2002).
2. I. Eschrich, in these Proceedings.
3. T. Hryn'ova, in these Proceedings.